THE ASTROPHYSICAL JOURNAL, 386:618–626, 1992 February 20

A CO STUDY OF SHARPLESS 171: EVIDENCE FOR INTERACTION BETWEEN THE H II REGION AND ITS NEIGHBORING MOLECULAR CLOUD

JI YANG
Purple Mountain Observatory, Academia Sinica, Nanjing 210008, China
AND
YASUO FUKUI
Department of Astrophysics, Nagoya University, Chikusa-ku, Nagoya 464-01, Japan
Received 1990 August 21; accepted 1991 July 10

ABSTRACT

Observations of the S171 region were made using the $J = 1$–0 lines of ^{12}CO, ^{13}CO, and $C^{18}O$ emission. The large-scale molecular gas distribution in S171 and its neighborhood has been mapped. Two dense molecular clumps have been revealed near the young star cluster Be 59 in the central region of S171. The mass of these clumps is estimated in total to be 600 $M_\odot$. A comparison with radio continuum observations shows that the dense gas is contacting with the continuum source. Spectra of ^{13}CO and $C^{18}O$ exhibit highly asymmetric shapes, indicating that the dense clumps are suffering dynamic disturbance due to the H II region. The disturbed gas component of one of the clumps shows good correspondence with the luminous ridge of the continuum emission. The interpretation is made that ionization fronts generated by the nearby star cluster drive shocks into the molecular clumps. The evolutionary effects of the molecular clumps under the ionization field of massive stars in the region are discussed.

Subject headings: H II regions — ISM: individual (Sharpless 171) — radio lines: molecular: interstellar

1. INTRODUCTION

Interactions between newly formed H II regions and their parental molecular clouds are the natural consequence of massive star formation. In this way, the surrounding material is dispersed and the newly formed stars become visible. Many efforts have been devoted to observing such interactions by molecular line spectroscopy (e.g., Lada et al. 1978; Elmegreen & Moran 1979; Loren 1979; Thronson, Lada, & Hewagama 1985; Sugitani et al. 1986; Keto & Ho 1989). Some evidence has been presented showing that molecular material near H II regions may be disturbed by several kilometers per second (see, e.g., the review by Elmegreen & Wang 1988). The processes of shock excitation and the evolution of remnant clouds, however, have not been studied in enough detail. With appropriate sources observed, comparison of the observed facts with those predicted by theories becomes more feasible.

Sharpless 171 is a large H II region and is the main cloud associated with the Cepheus OB4 stellar association. Optical emission of the H II region, centered at $l = 118°$ and $b = 5°$, can be traced to a size of $\sim 3° \times 3°$ from the Palomar Observatory Sky Survey (POSS) prints. The association includes more than 10 stars earlier than type B1. A star cluster, Be 59, containing one O7 and several of later types, is located at the central portion of the nebulous region. Ages of these stars are in the range (2–6) $\times 10^5$ yr (Cohen & Kuhi 1976). The distance to the region is 850 pc (MacConnell 1968). An extensive summary of previous optical observations has been given by Lozinskaya, Sitnik, & Toropova (1987).

Properties of the ionized gas near the central star cluster Be 59 have been investigated by many authors in radio continuum and recombination lines (e.g., Felli, Habing, & Israel 1977; Rossano, Angerhofer, & Grayzeck 1980; Harten et al. 1981; Matthews 1982). Weak, diffuse continuum emission appears over nearly the whole optical H II region, according to Rossano et al. (1980). An enhanced continuum source, designated as G118.1 + 5.0 by Felli et al. (1977), was found on the east side of Be 59, which appears upon the weak diffuse emission. A prominent ridge structure of enhanced radio emission is associated with the western periphery of the continuum source, where no pointlike radio source has been found to be physically associated with the continuum ridge (Harten et al. 1981).

In an earlier CO study, Elmegreen, Dickinson, & Lada (1978) observed a bright-rimmed molecular cloud, NGC 7822, which is located at the northern edge of the S171/NGC 7822 region (see also Wootten et al. 1983). Most of the H II region, however, has not yet been observed in molecular lines. Recently, Leisawitz, Bash, & Thaddeus (1989) reported a CO ($J = 1$–0) survey of a $3° \times 3°$ area in S171 with a beam size of 8′.7. Near Be 59 in the central part of the H II region, they detected emission at $V_{LSR} = -20$ to -15 km s^{-1}, while its structure was not resolved. Liu et al. (1988) observed an area $9' \times 9'$ centered at the star cluster Be 59 in ^{13}CO ($J = 1$–0). They also found strong emission at $V_{LSR} = -14$ km s^{-1} at the western part of Be 59. The distribution and detailed structure of the dense gas have not been clearly revealed.

We carried out a large-scale survey of molecular clouds over the whole H II region. In this paper we present observational results of the S171 region obtained from the ^{12}CO, ^{13}CO, and $C^{18}O$ ($J = 1$–0) lines. The large-scale ^{13}CO mapping is included in a large-scale survey of star-forming regions along the Galactic plane (Fukui 1988, 1989; Fukui et al. 1986, 1989, 1990), including the Cepheus-Cassiopeia region (Yang et al. 1990, 1991), with the 4 m telescope at Nagoya University. Details of the observational methods are described in § 2. In § 3 the general distribution of molecular gas in S171 is briefly described. We then concentrate on the study of dense gas revealed from the central part of the H II region. We give observational evidence for the interactions between the H II region and the molecular clumps in § 4. We also discuss the

effect and consequence of the interaction. The major characteristics indicated by the observations will be summarized in § 5.

2. OBSERVATIONS

Observations of ^{12}CO, ^{13}CO, and $C^{18}O$ ($J = 1$–0) transition lines were made with the 4 m telescope at Nagoya University within the period from 1988 December to 1989 May. A general description of the telescope is given by Kawabata et al. (1985). A 4 K cooled SIS mixer receover was installed, which provided system temperatures between 150 and 250 K (double sideband). The beam size was 2.'7 at 110 GHz. Spectral data were obtained with a 1024 channel acousto-optical spectrometer having a frequency resolution of 40 kHz (corresponding to a velocity resolution of 0.11 km s^{-1} at 110 GHz). Antenna temperature was scaled following the standard chopper-wheel method (Kutner & Ulich 1981). The image sideband of our receiver system was not completely suppressed, resulting in slight elevation dependence of the antenna gain. Elimination of such an effect was accomplished by observing S140 and fitting the antenna temperature to an exponential law of atmospheric extinction. Source antenna temperature was further calibrated by referring to the intensities of S140 to be 20 K in ^{12}CO and 6 K in ^{13}CO, respectively.

A layout of grid points at different spacings is shown in Figure 1*a*. A large-scale ^{13}CO mapping, which extends over the range $l = 115°$–$125°$ and $b = 0°$–$10°$, was made at 8′ spacing. The whole area shown in Figure 1*a* was observed in this mapping. Area B covers a major portion of the H II region at 4′ spacing. Area C was mapped in 2′ grid spacing in $J = 1$–0 transitions of both the ^{12}CO and ^{13}CO, which fully covered the area of intense molecular emission. All the ^{12}CO data were obtained in position-switching mode. Mapping in ^{13}CO was made in frequency-switching mode for areas A and B and in position-switching mode for area C. Toward the two ^{13}CO peak positions, $C^{18}O$ profiles were taken in position-switching mode. The rms noise level for ^{12}CO temperature is in the range 0.6–0.8 K. For ^{13}CO in areas A and B, the rms noise level is generally around 0.3 K, and in area C it is typically 0.2 K. Since the intensity of the $C^{18}O$ line is quite weak, we integrated down to an rms level of ~ 50 mK to ensure a signal-to-noise ratio of 5.

3. RESULTS

It is revealed from our mapping that molecular emission is extended over $\sim 3° \times 3°$ in the neighborhood of S171, as shown in Figure 1*b*. Emission features are generally clumpy and/or filamentary. Most of the emission features appear at V_{LSR} from 0 to -8 km s^{-1}. This component shows global coincidence with weak extinction features on POSS prints. The coverage of emission at this V_{LSR} is extended beyond the area shown in Figure 1*b*. It appears all over our surveyed area within the range $l = 115°$–$125°$ and $b = 0°$–$10°$, including M120.1 + 3.0, a newly discovered molecular cloud 3° southeast of the center of S171 (Yang et al. 1990), and L1287 (Yang et al. 1991). The general correspondence of this component with the extinction features, the lower V_{LSR}, and the large extension suggest that this component originates in the nearby molecular clouds. This component is also observed in a large-scale ^{12}CO ($J = 1$–0) survey at higher latitude in the second Galactic quadrant by Grenier et al. (1989). Within current survey observations, there is no clear evidence of physical connection between the -5 km s^{-1} component and the molecular clumps in the S171 region. In this work we will not deal with this component.

3.1. *Dense Molecular Clumps near the Young Star Cluster Be 59*

In the central part of S171, intense ^{13}CO emission is detected. From current ^{13}CO mapping, it is revealed that the emission comes from two major clumps. A ^{13}CO map, integrated from -18 to -10 km s^{-1}, is shown in Figure 2. The two clumps, designated as C1 and C2, are projected inside the inner area of the optical H II region. Both the clumps are located on the west side of Be 59. The peaks of the two clumps are separated by ~ 3 pc. The northeast clump, C2, is closer to Be 59. The projected separation from the ^{13}CO peak of C2 to Be 59 is ~ 2.5 pc. A secondary peak is recognized in the south protrusion of the clump C2. The area observed by Liu et al. (1988) clearly corresponds to part of the eastern boundary of this secondary peak. The extension of the protrusion of C2 results in an overlap of the two clumps as shown in Figure 2, while it is not clear that the two major components are spatially connected.

Line profiles of ^{12}CO and ^{13}CO from the peak positions of C1 and C2 are shown, respectively, in the upper and lower panels in Figure 3*a*. The low-intensity velocity feature peaked at -8 km s^{-1}, as pointed out above, comes from the foreground gas component. Besides this component, two major features can be distinguished from the intense parts of the ^{13}CO profiles in each panel. These features include a narrow, peaked component and a broad plateau component. For the clump C1, the narrow component appears at $V_{LSR} = -13$ km s^{-1}. The broad plateau component is traceable down to -18 km s^{-1} at the low-velocity end. For the clump C2, a narrow component centered at $V_{LSR} = -16$ km s^{-1}, as well as a plateau component extended to the high-velocity end, is recognized. The plateau components are also present in the $C^{18}O$ profiles as shown in Figure 3*b*. In the case of C1, the plateau component is clearly recognized down to more than 2 km s^{-1} to the blueshifted side in the $C^{18}O$ profile.

The ratios of $T_R^*(^{13}CO)$ to $T_R^*(C^{18}O)$ at line centers are 11:13, respectively, for both the emission peaks of the two clumps. These ratios are comparable to those derived from other molecular clouds associated with H II regions (e.g., Taylor & Dickman 1988). Under the assumption of local thermal equilibrium (LTE) and adopting equal T_{ex} for ^{12}CO, ^{13}CO, and $C^{18}O$ ($J = 1$–0) transitions, it can be shown that the $C^{18}O$ optical depths are ~ 0.02 at line centers for both the peaks, and the ^{13}CO optical depths are 0.2–0.3. For both the clumps, the results indicate that the plateau components are not caused by self-absorption, and, instead, they represent velocity fields different from that represented by the narrow components.

The narrow and the plateau components are illustrated by a position-velocity diagram in Figure 4. Data points for this diagram are adopted along the line (marked in Fig. 2 by I–I′) linking the star cluster Be 59 and the peak of C1. It is clear from the diagram that the plateau component is a disturbed gas component superposed upon a quiescent component. The disturbed component is restricted to a small area at the eastern edge of C1 and has a linear size somewhat smaller than 9′ or 2.2 pc at a distance of 850 pc. This component is extended to ~ 4 km s^{-1} relative to the quiescent one.

The distribution of the narrow and the plateau components, separated by integration within different velocity intervals, is shown in Figure 5. The rest component of C2 and its secondary peak can be identified as the feature in the northeast part of Figs 5*a* and 5*b*. The plateau component, which is elongated in

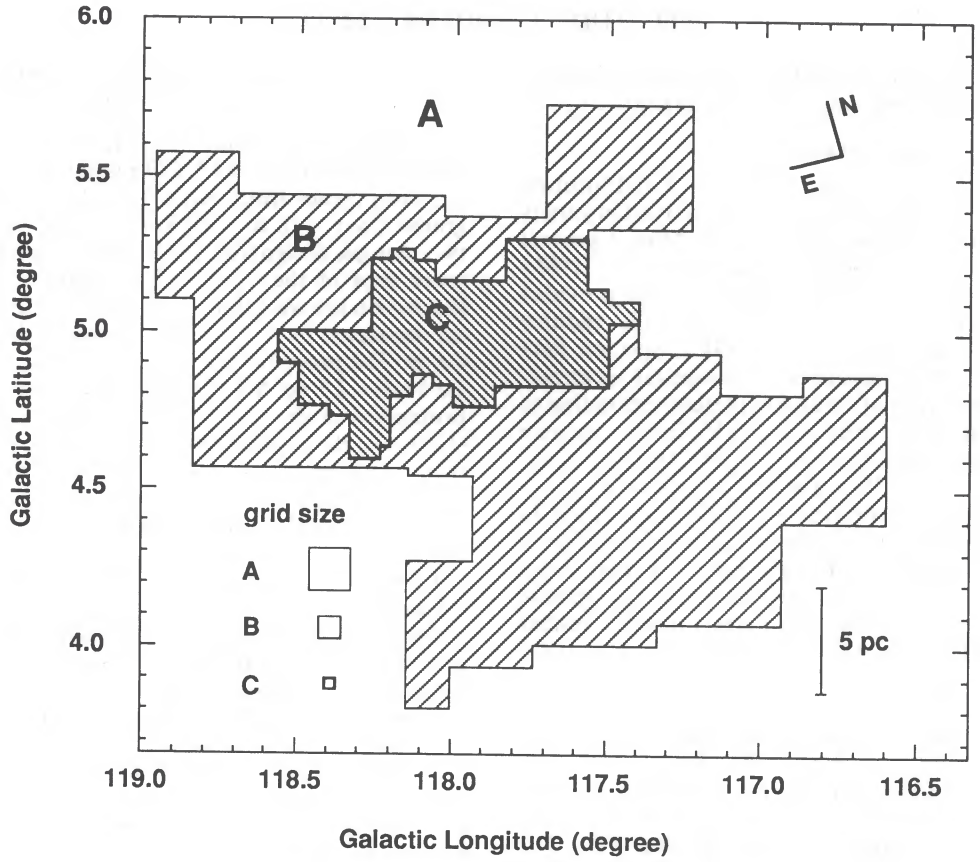

FIG. 1*a*

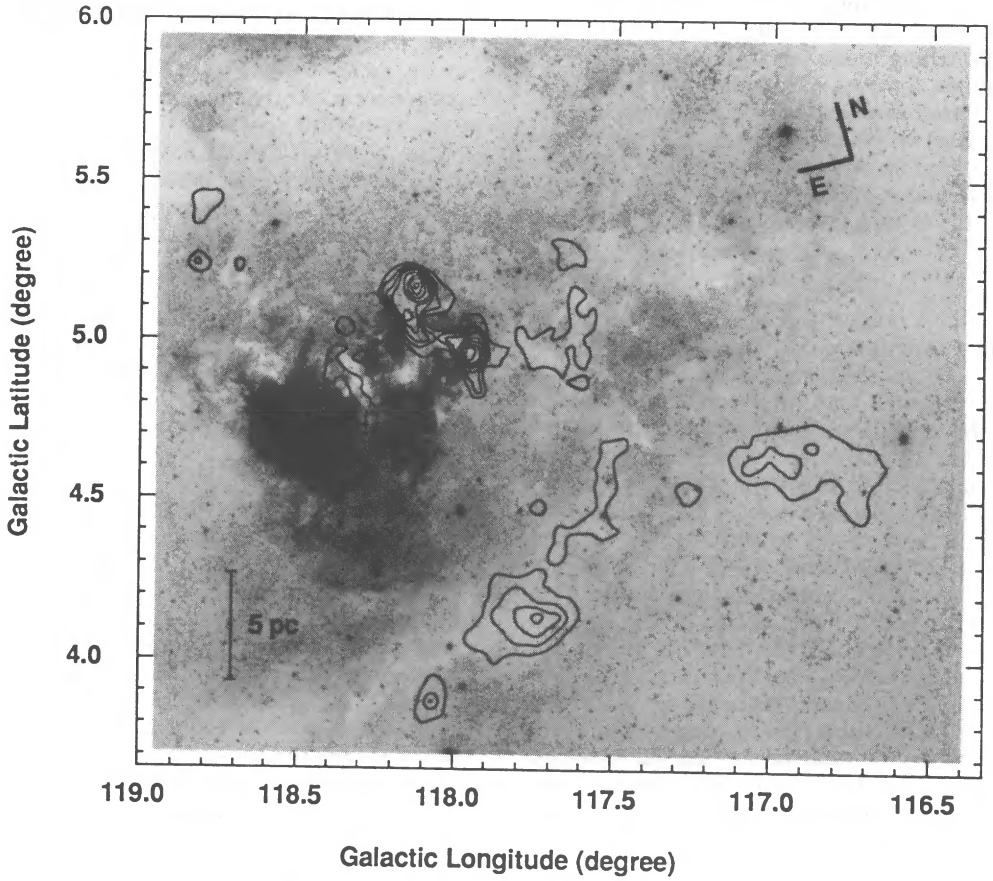

FIG. 1*b*

FIG. 1.—(*a*) Overlay of mapping coverage of S171 in Galactic coordinates. (*b*) Contour map of ^{13}CO integrated intensity of S171 region over all the observed velocity range from -25.0 to 0.0 km s^{-1}, superposed upon the POSS red print. Contour levels begin from 1.5 K km s^{-1} with increments of 1.0 K km s^{-1}.

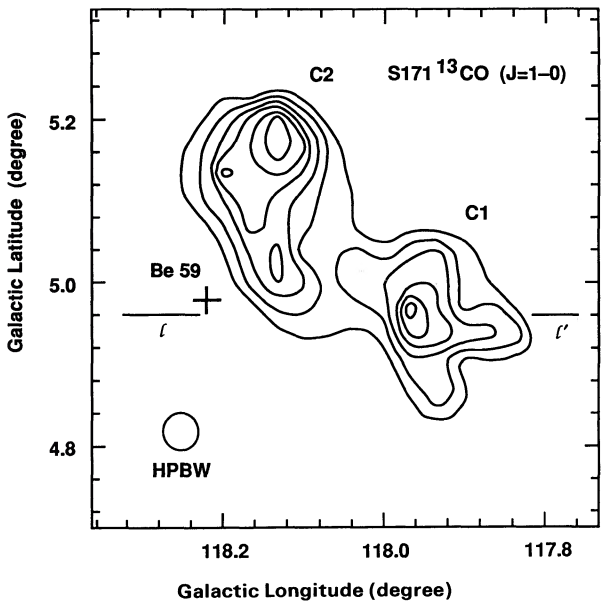

FIG. 2.—Contour map of ^{13}CO integrated intensity over the velocity range from -18.0 to -10.0 km s^{-1}. The lowest level and increments are 1.5 K km s^{-1}. The relative positions of the two clumps, C1 and C2, are labeled. The location of the star cluster Be 59 is marked by a cross. The line l–l′ illustrates the cut direction for the *p-v* map in Fig. 4.

the northeast to southwest direction, forms a wall facing Be 59. This wall remains recognizable as the feature in the northeast part in Fig. 5*d*. The plateau component of C1, which is most obvious in Fig. 5*c*, exhibits a clear and slightly curved front structure in the vertical direction relative to Be 59. It is characteristic that both the rest components of the two clumps are located on the far sides from Be 59. The rest component of C2 is more prominent. It may be due to the larger size and mass of the clump, which will be discussed in the next paragraph.

3.2. *Mass Estimates for the Dense Molecular Clumps*

Each profile involves both the narrow and the plateau components. Before the masses of different components are estimated, it is necessary to separate them from each other. It is reasonable to consider that the intrinsic profiles of the narrow components are Gaussian. The exact profiles of the plateau components depend on the relative contributions of emitting material at different velocities. In an approximate way, we fit the CO and ^{13}CO profiles to two Gaussian components. Values from the two peak positions are listed in Table 1A. Under the assumption of LTE, we calculated the masses of the two clumps for each component. The excitation temperature T_{ex} comes from the peak radiation temperature of ^{12}CO of each component when the line is assumed to be optically thick. The abundance ratio of H_2 to ^{13}CO is adopted to be 5×10^5 (Dickman 1978). In the calculation, the sizes of the narrow and plateau components of each clump were adopted to be the same, estimated from the full widths at the half-maximum

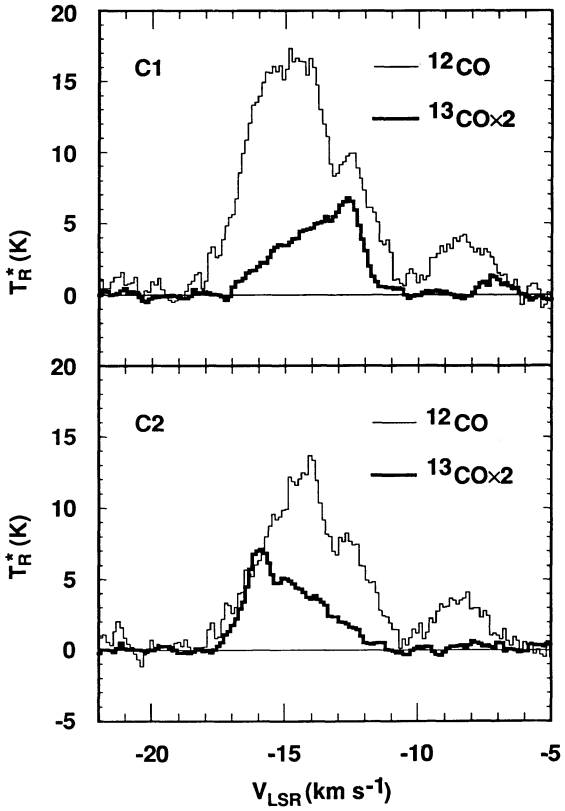

FIG. 3*a*

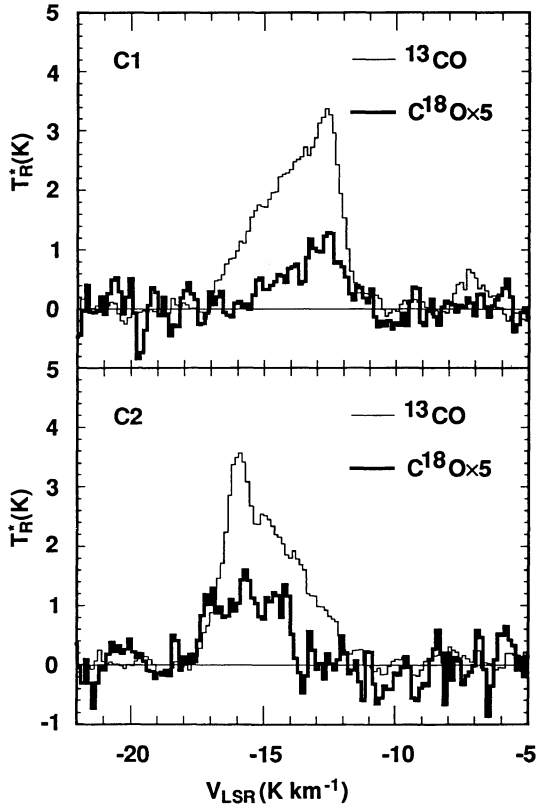

FIG. 3*b*

FIG. 3.—(*a*) Spectra of ^{12}CO (*thin lines*) and ^{13}CO (*thick lines*) from the peak positions of clumps C1 [R.A.(1950) = $23^h57^m49^s.9$ decl. = +67°03′36″] and C2 [R.A.(1950) = $23^h58^m26^s.1$, decl. = 67°17′20″]. Intensities of ^{13}CO are enlarged by a factor of 2. (*b*) Spectra of ^{13}CO (*thin lines*) and $C^{18}O$ (*thick lines*) from the same positions as in (*a*). The $C^{18}O$ intensities are enlarged by a factor of 5.

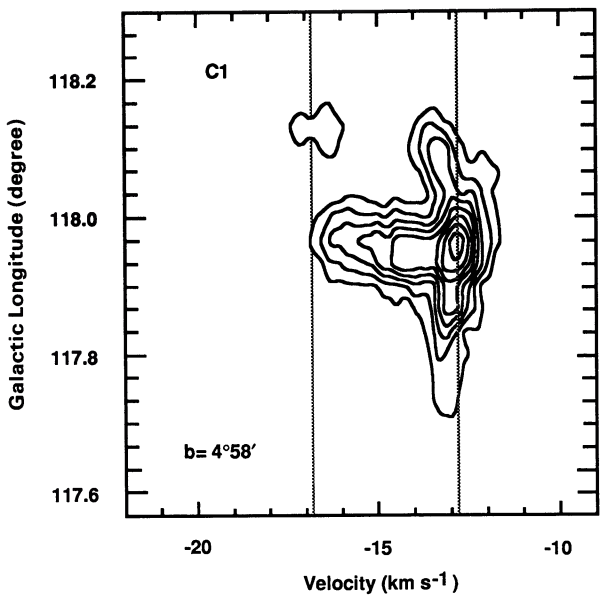

FIG. 4.—Position-velocity diagram from the clump C1 cut along constant Galactic latitude ($b = 4°58'$), as is illustrated in Fig. 2 by the line I–I′. Contours and increments are 0.3 K. The velocity resolution is 0.1 km s^{-1}, and the spatial resolution is 2′.7.

TABLE 1A

OBSERVED PARAMETERS OF MOLECULAR CLUMPS IN S171

	C1		C2	
PARAMETERS	Narrow	Plateau	Narrow	Plateau
$T_R^*(^{12}CO)$ (K)	5.1	16.9	13.8	12.3
$T_R^*(^{13}CO)$ (K)	1.8	2.4	1.9	2.4
$V_{LSR}(^{13}CO)$ (km s^{-1})	−12.6	−14.0	−14.8	−16.0
$\delta V(^{13}CO)$ (km s^{-1})	1.0	3.4	0.9	3.3
Size (pc × pc).....	2.0 × 1.0	2.0 × 1.0	3.0 × 1.5	3.0 × 1.5

TABLE 1B

DERIVED PROPERTIES OF MOLECULAR CLUMPS IN S171

	C1		C2	
PARAMETERS	Narrow	Plateau	Narrow	Plateau
T_{ex} (K)	8.3	20.3	17.2	15.7
τ^{13}	0.44	0.15	0.15	0.22
N^{13} ($\times 10^{15}$ cm^{-2})	2.1	12.0	2.2	11.0
$n(H_2)$ (cm^{-3})	3.5×10^2	2.0×10^3	2.5×10^2	1.1×10^3
M ($M_\odot$)	30	166	70	320

NOTE.—The number density $n(H_2)$ is derived from the peak column density and the minimum elongation of each clump.

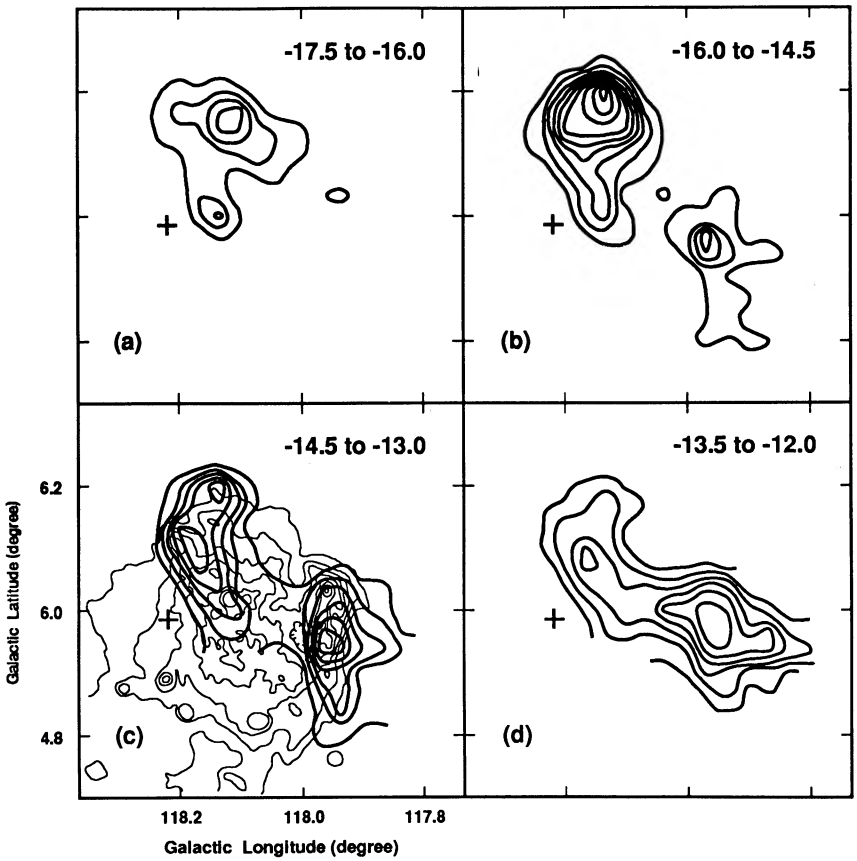

FIG. 5.—(*a–d*) Intensity maps of ^{13}CO integrated in different velocity ranges. The four panels are separated in velocity intervals of 1.5 km s^{-1}. Both the lowest level and the increments are 0.5 K km s^{-1} in all four panels. Each panel shows the same coordinate range as in Fig. 2. The small crosses denote the position of Be 59. A contour map of the 0.61 GHz radio continuum emission of S171 traced from Harten et al. (1981) is superposed upon the ^{13}CO contours in (*c*).

levels of the integrated intensity distribution. The results are presented in Table 1B. The total molecular mass in the two ^{13}CO clumps is estimated to be $\sim 600\ M_{\odot}$. The clump C2 has twice the mass of C1, which is mainly due to the large size of C2.

Estimates of column densities based on the ground-level CO transitions and on the hypothesis of LTE may involve some uncertainties in this case. The possible sources of error are the nonuniformity of the temperature distribution within each clump, the uncertainty in the determination of the emission area of each component, and the unknown filling factors. Since most of the ^{13}CO luminosity comes from the plateau components, we do not expect the above uncertainties involved in the narrow components to be of a large fraction. Besides, an uncertainty may come from the fractional abundance of ^{13}CO, but its possible range is within a factor of 2, as suggested by the ratios of optical depths of ^{13}CO to C^{18}O, which is equivalent to an isotopic abundance ratio twice as high as the terrestrial value of 5.5.

4. DISCUSSION

4.1. *Relationship between the Molecular Clumps and the* H II *Region*

Evidence for the association of the clumps with the star cluster is provided by the radial velocity measurement of the member stars of Be 59 (Liu et al. 1989). The radial velocity of Be 59, $V_{LSR} = -15.7$ km s^{-1}, is within the velocity range between $V_{LSR} = -14.4$ and -16.0 km s^{-1} for the clumps C1 and C2, indicating that the dense molecular clumps are associated with Be 59.

A weak, diffuse continuum source, which has almost the same size as the optical H II region of S171, was observed by Rossano et al. (1980). The flat spectral index of the diffuse emission indicates the thermal nature of the source. Inside the diffuse medium an extended continuum source G118.1+5.0 was revealed (Felli et al. 1977; Harten et al. 1981). The bulk of this source (having a size of 15′ above the contour of 35 mJy per beam in Fig. 2 of Harten et al. 1981) is located on the west side of Be 59. Two major components can be distinguished from this continuum source. The southwest boundary of the continuum source is very sharp. Parallel to the boundary, there is a prominent radio ridge upon the continuum source elongated nearly in the north-south direction, as noted by Harten et al. (1981). The reality of this ridge has been confirmed by observation with the Very Large Array (Rossano, Grayzeck, & Angerhofer 1983).

For comparison of the CO results with those of the continuum, gray-scale maps of the ^{13}CO integrated intensity and ^{12}CO peak intensity of the clumps are superposed upon the 0.61 GHz continuum map of Harten et al. (1981) in Figures 6*a* and 6*b*, respectively. The two clumps of molecular emission show general correlation with the far-side boundaries of the continuum source, and each molecular clump corresponds to a radio enhancement feature in G118.1+5.0. The elongation of C1 marches with the sharp boundary of the westernmost arc and is nearly parallel to the radio ridge. The peak of C1 is coincident with the peak of the continuum enhancement.

The high-degree spatial correlation between the ionized and the molecular gas suggests that they are physically associated. The sharp boundary of the continuum emission is probably due to physical confinement by the molecular gas. The Lyman continuum photons from stars in Be 59 ionize molecular gas of the two clumps on their near-side surfaces. Over the weaker parts of the continuum source, there is clearly no associated molecular emission. It can be naturally explained that the extension of the continuum emission to the east of the two enhancements is caused by the flow of ionized gas dispersing away from the surfaces of the molecular clumps.

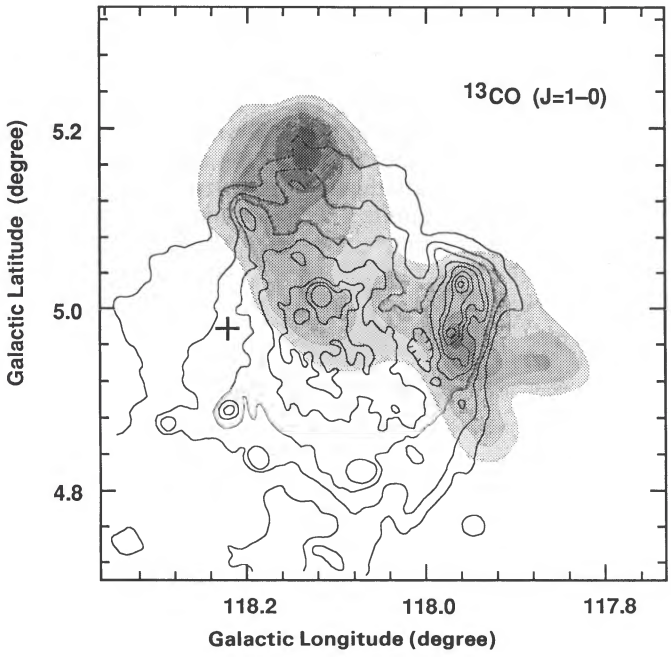

FIG. 6*a*

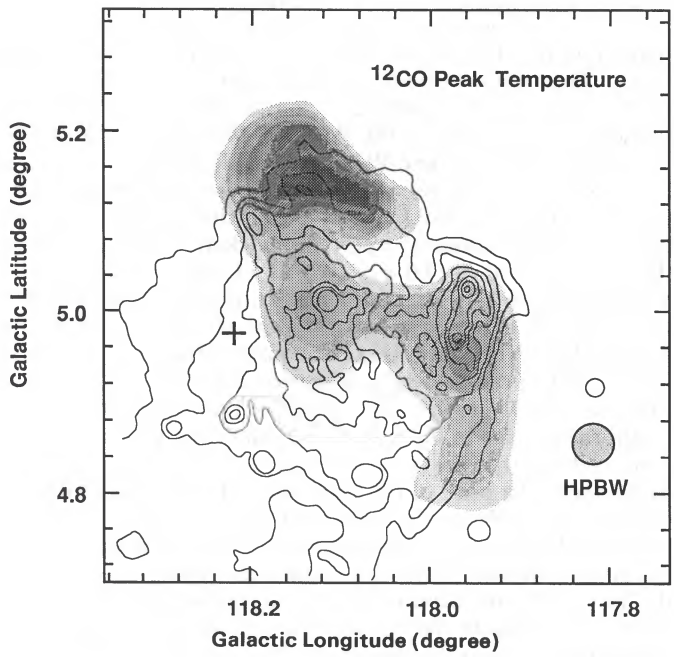

FIG. 6*b*

FIG. 6.—(*a*) Gray-scale map of ^{13}CO integrated intensity superposed upon a contour map of the 0.61 GHz radio continuum emission. The lowest level and increments of the gray scales are 1.5 K km s^{-1}. (*b*) Gray-scale map of ^{12}CO peak radiation temperature superposed upon the 0.61 GHz radio continuum map. The gray-scale levels begin from 6 K with increments of 2 K.

Similar to that of ^{13}CO, the ^{12}CO peak temperature distribution shows good correspondence with the continuum emission as shown in Figure 6*b*. The overall sizes of the ^{12}CO emitting areas are comparable to their ^{13}CO counterparts, further suggesting that these clumps are not very extended beyond the ^{13}CO boundaries defined by the lowest contour levels in Figures 2 and 6*a*. The morphology of C1 in ^{12}CO is slightly different from that in ^{13}CO in the sense that the ^{12}CO peak temperature distribution tends to delineate the sharp boundary of the continuum source. The secondary peak of C2 becomes more obvious in ^{12}CO. This tendency is consistent with the possibility that the ^{12}CO peak temperature reflects the effective side illumination of the clumps by the cluster members.

On the basis of the physical association of the molecular clumps, the star cluster, and the ionized gas, it is possible to examine the nature of the internal motion of the molecular clumps reflected by the unusual line profiles presented in § 3, the origin of the ionized gas, and the evolution of the whole complex.

4.2. *Nature of the Velocity Field in the Molecular Clumps*

When ionization occurs, shock fronts will be generated (Spitzer 1968). Propagation of the shock perturbation into molecular clumps gives one possibility of raising the plateau components. The electron density averaged over G118.1+5.1 is ~ 30 cm^{-3}. At the position of the radio ridge, it is estimated to be 40 cm^{-3} (Harten et al. 1981). Adopting 3.5×10^2 cm^{-3} as the number density for the undisturbed molecular gas and assuming the temperature of the ionized gas to be 1×10^4 K, the ratio of the pressure of ionized gas, P_i, to that of neutral gas, P_c, is estimated to be as high as 100. The shock driven by the pressure gradient is expected to have a velocity $V_s = (\eta P_i/\rho_c)^{1/2}$, where ρ_c is the mass density of neutral (molecular) gas. The factor η equals 2 for a D-critical ionization front (Elmegreen & Lada 1977). The adopted parameters give $V_s = 3$ km s^{-1}, which is close to the observed value of 4 km s^{-1}, suggesting that the plateau component is mainly raised by the shock. The shock velocity estimated here is comparable to those from other molecular clouds such as NGC 281 (Elmegreen & Moran 1979), W3, W4, W5 (Lada et al. 1978; Thronson et al. 1985), and W33 (Keto & Ho 1989).

To examine the relationship between the shocked gas components and the radio features, we plotted contours of 0.61 GHz continuum intensity upon the shocked ^{13}CO component ($V_{LSR} = -14.5$ to -13.0 km s^{-1}) in Figure 5*c*. The clearest correspondence between the plateau component and the radio continuum distribution comes from the clump C1, as favored by the edge-on orientation of the configuration relative to the line of sight. It can be easily recognized that the vertical wall of shocked ^{13}CO emission is oriented almost parallel to the bright radio ridge in the case of the clump C1, which provides clear evidence that the ridge and the shock front are contacting each other. The peak of C1 approximately coincides with the concavity seen from the west boundary of the continuum, where molecular gas of the narrow component is more accumulated. Detailed morphology and the velocity field around the peak position deserve further high-resolution studies in order to investigate the fine structure of the molecular shock. Indication of the correspondence between the shocked gas elongation and the continuum enhancement can also be traced from C2, especially at the southern half of C2, where the elongated emission changes to a direction perpendicular to Be 59 and forms a clear wall.

Models concerning the shock compression of molecular gas predict that a neutral clump can be compressed either laterally (Elmegreen & Lada 1977) or spherically (Klein, Whitaker, & Sandford 1985). It has been shown that for a clump of several solar masses located near an O-type star, the ionizing flow generates a shock front surrounding nearly the whole surface of the clump, and the shock front tends to focus toward the center of the clump, according to the calculations of radiative implosion by Klein et al. (1985). From the relative distribution of the shocked and quiescent gas components in the clumps, it is rather clear that the compression of molecular clumps in S171 is lateral rather than spherical. Therefore, for molecular clumps of higher masses as observed here, it is obvious that the shock front tends to show a slab structure similar to that of the propagating ionization front discussed by Elmegreen & Lada (1977).

Adopting 1 pc as the size of C1 and 4 km s^{-1} as the shock velocity, the shock crossing time over the molecular clumps is 5×10^5 yr. The time scale is comparable to the age estimate of Be 59, suggesting that the excitation of the shock fronts began almost simultaneously with the ignition of massive stars in Be 59. This is consistent with the fact that the shock-disturbed gas shows significant ^{13}CO emission as observed.

4.3. *Evolution of the Molecular Clumps in the* H II *Region*

Exposed to the radiation field of the young star cluster, the molecular clumps will be evaporated as a result of the ionization by the Lyman continuum photons. The total Lyman continuum luminosity from Be 59 and the immediate neighborhood of the two clumps, N_L, is estimated in Table 2, where we have used spectroscopic data from MacConnell (1968) and the Lyman continuum luminosity of each spectral type by Panagia (1973). The total rate is 6.5×10^{48} photons s^{-1}. Attenuation of the ionizing flux by recombination along the path between the cluster and the surface of the clumps is estimated under the spherical dispersion approximation for the ionization ejecta (Spitzer 1968), i.e., assuming that the ionized gas density decreases as r^{-2} from the surface of the clumps. The ionized gas leaves the ionization front at a velocity of the sound speed of the ionized gas, $C_{s,i}$. If $F_0 (= N_L/4\pi d^2)$ denotes the Lyman continuum flux at the position of a clump without attenuation, where d is the distance of the clump to Be 59, and F_1 is the flux under attenuation, an attenuation factor $f = F_0/F_1$ can be defined (Spitzer 1968). When f is much greater than unity, it can be estimated from $f = (\alpha F_0 R_c/3C_{s,i}^2)^{1/2}$, where α is the recombination rate, 2.6×10^{-13} cm^3 s^{-1} at $T = 10^4$ K

TABLE 2

STELLAR CONTENTS AND CORRESPONDING LYMAN CONTINUUM FLUXES

Star	Spectral Type	N_L (photons s^{-1})
2	B1	1.95×10^{45}
3	O9	1.05×10^{48}
11	B1	1.95×10^{45}
12	B1	1.95×10^{45}
13	B0	2.29×10^{47}
14	O7	4.17×10^{48}
15	B3	4.90×10^{43}
28	B2	4.47×10^{44}
29	O9	1.05×10^{48}
Total	...	6.5×10^{48}

NOTE.—Numbers of stars follow Table 1 in MacConnell 1968; the Lyman continuum fluxes are ZAMS values.

(Mathews 1969), and R_c is the radius of a molecular clump. In the case of C1, where the distance to Be 59 is ~ 3 pc and the radius is ~ 2 pc defined by the major elongation, f can be evaluated to be 60. The mass-loss rate due to ionization, $\dot{M}$, is estimated from $\dot{M} = \pi R_c^2 m_H (F_0/f)$, where m_H is the atomic mass of hydrogen. The mass-loss rate of C1 is estimated to be $2 \times 10^{-4}\ M_\odot\ \mathrm{yr}^{-1}$. The characteristic evaporation time scale τ_{ev} derived from the core mass M_c is $\sim M_c/\dot{M}$, or 1×10^6 yr. The mass of ionized gas of G118.1+5.0 can be estimated to be $\sim 140\ M_\odot$, adopting the size of 15′ and a mean electron density of 30 cm^{-3}. This mass is comparable to the mass-loss rate of the clumps (about double that of C1) multiplied by the age of Be 59, which confirms the possibility that the bulk of the ionized gas originated in the molecular clumps.

The evaporation time scale of the molecular clumps is close to the free-fall time scale of the compressed molecular gas, $\tau_{ff} = 3 \times 10^7\ n(H_2)^{-1/2}$, or 7×10^5 yr. Bearing in mind the possible range of uncertainties in deriving molecular gas densities and masses, we suggest two different possibilities concerning the ultimate fate of the molecular clumps, since either they will be evaporated, or inside them a second generation of stars can be formed from the postshock gas. As the shock penetrates into the molecular clumps, it forms a compressed gas layer which is unstable against self-gravity (Elmegreen 1989). One can expect that a new generation of stars will eventually be formed from the compressed gas layer. For large and massive clumps, this process is similar to the propagational star formation proposed by Elmegreen & Lada (1977). Furthermore, the combination of ionization evaporation and acceleration may cause the molecular clumps to lose masses and gain high speeds. The clumps studied here may evolve into somewhat similar stages to those bright-rimmed globules studied by Reipurth (1983) and Sugitani et al. (1989), which have lower masses and high escaping velocities and exhibit some evidence for star formation triggered by implosive shocks.

The propulsion by the ejection of ionized gas from the clumps will accelerate the clumps away from the star cluster. This mechanism, which is sometimes called the "rocket effect," was originally discussed by Oort & Spitzer (1955) and more recently by Bertoldi (1989). To examine whether the mechanism is effective in the current situation, we again discuss the case for the clump C1. The rest component of C1 is -12.6 km s^{-1}, 3.1 km s^{-1} different from the radial velocity of Be 59. Supposing that this velocity difference is caused by acceleration, during a period of the age of Be 59, (2–6) $\times 10^5$ yr, the displacement is expected to be within the range of 0.5–2 pc. Under the assumption that C1 was initially at rest, it can be estimated from the simple rocket equation $m = m_0 \exp(-V/C_{s,i})$ that to gain a velocity $V = 3$ km s^{-1} the clump would have to lose 30% of its mass during the past ionization acceleration. Since the projected separation between Be 59 and C1 is ~ 3 pc, the above estimate is consistent with the possibility that the clumps originated near Be 59, that is, they represent part of the parental cloud from which the cluster was formed.

5. SUMMARY

To summarize the results and the related interpretations made in this paper, we propose a schematic model of S171 in Figure 7. The star cluster Be 59 was once formed inside a molecular cloud. After the formation of the cluster, the Lyman continuum photons from the massive stars soon ionized the less dense regions of the cloud, forming a large, diffuse envelope of lower electron densities. The denser parts $[n(H_2) > 10^2]$ of the parental molecular clouds survived several times 10^5 yr after the cluster formation. The Lyman continuum photons from the member stars illuminate the near-side surfaces of these clumps and excite ionization fronts. Flows of ionized gas from these surfaces disperse and are observed as continuum sources of higher electron densities. In the close vicinities of these ionization fronts where ion and electron densities are further enhanced, radio continuum ridges are observed. The high pressure of ionized gas drives shocks into the molecular clumps at velocities of up to 4 km s^{-1}. The clumps are compressed laterally by the shocks. Emission from the compressed material is observed as the plateau components in ^{13}CO and $C^{18}O$ line spectra. The acceleration force has not pushed the clumps far away from their original positions and has not fed them with high acceleration velocities, as argued by the small differences among the radial velocities of molecular clumps and of the star cluster. Because of ionization, the clumps are losing mass at a rate of 10^{-5} to $10^{-4}\ M_\odot\ \mathrm{yr}^{-1}$. It is generally uncertain whether the clumps will collapse, and form the next generation of stars, or will be evaporated within the next 10^6 yr.

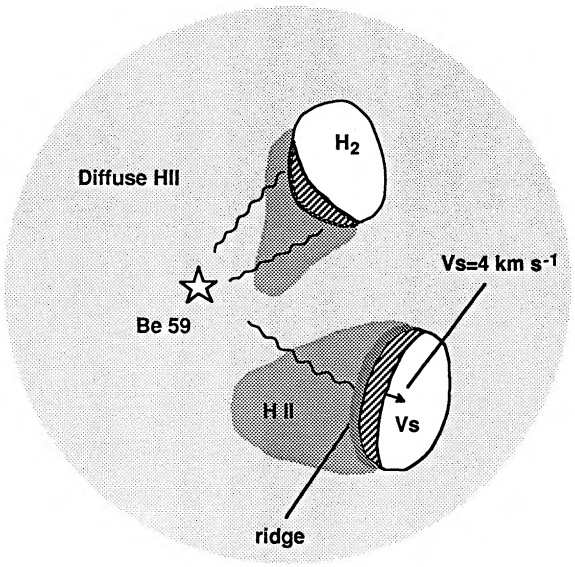

FIG. 7.—Schematic model derived from the observed properties of molecular clumps inside S171.

We are grateful to H. Ogawa and A. Mizuno for their excellent work in making the high-sensitivity SIS mixer receiver for the 4 m telescope at Nagoya University. We benefited from various discussions with K. Sugitani. It is a pleasure to thank our referee, B. G. Elmegreen, for his helpful comments on this paper. One of us, J. Y., would like to acknowledge Inoue Foundation for awarding a fellowship. This work is supported in part by a Grant-in-Aid for Scientific Research of the Ministry of Education, Science, and Culture, Japan (Nos. 62640002, 63611511, and 01065002).

REFERENCES

Bertoldi, F. 1989, ApJ, 346, 735
Cohen, M., & Kuhi, L. 1976, ApJ, 210, 365
Dickman, R. L. 1978, ApJS, 37, 407
Elmegreen, B. G. 1989, ApJ, 340, 786
Elmegreen, B. G., Dickinson, D. F., & Lada, C. J. 1978, ApJ, 220, 853
Elmegreen, B. G., & Lada, C. J. 1977, ApJ, 214, 725
Elmegreen, B. G., & Moran, J. M. 1979, ApJ, 227, L93
Elmegreen, B. G., & Wang, M. 1988, in Molecular Clouds in the Milky Way and External Galaxies, ed. R. L. Dickman, R. L. Snell, & J. S. Young (Berlin: Springer), 240
Felli, M., Habing, H. J., & Israel, F. P. 1977, A&A, 59, 43
Fukui, Y. 1988, Vistas Astr., 31, 217
———. 1989, in Proc. ESO Workshop on Low Mass Star Formation and Pre–Main Sequence Objects, ed. B. Reipurth (Garching: ESO), 95
Fukui, Y., Iwata, T., Mizuno, A., Bally, J., & Lane, A. P. 1990, in Protostars and Planets III (Tucson: Univ. Arizona Press), in press
Fukui, Y., Iwata, T., Takaba, H., Mizuno, A., Ogawa, H., Kawabata, K., & Sugitani, K. 1989, Nature, 342, 161
Fukui, Y., Sugitani, K., Takaba, H., Iwata, T., Mozuno, A., Ogawa, H., & Kawabata, K. 1986, ApJ, 311, L85
Grenier, I. A., Lebrun, F., Arnaud, M., Dame, T. M., & Thaddeus, D. 1989, ApJ, 347, 231
Harten, R. H., Goss, W. M., Matthews, H. E., & Israel, F. P. 1981, A&A, 103, 50
Kawabata, K., Ogawa, H., Fukui, Y., Takano, T., Fujimoto, Y., Kawabe, R., Sugitani, K., & Takaba, H. 1985, A&A, 151, 1
Keto, E. R., & Ho, P. T. P. 1989, ApJ, 347, 349
Klein, R. I., Whitaker, R. W., & Sandford, M. T., II. 1985, in Protostar and Planets II, ed. D. C. Black & M. S. Matthews (Tucson: Univ. Arizona Press), 33
Kutner, M. L., & Ulrich, B. L. 1981, ApJ, 250, 341
Lada, C. J., Elmegreen, B. G., Cong, H., & Thaddeus, P. 1978, ApJ, 226, L39
Leisawitz, D., Bash, F. N., & Thaddeus, P. 1989, ApJS, 70, 731
Liu, T.-X., Janes, K. A., Bania, T. M., & Phelps, R. L. 1988, AJ, 95, 1122
Loren, R. B. 1979, ApJ, 234, L207
Lozinskaya, T. A., Sitnik, T. G., & Toropova, M. S. 1987, Soviet Astron., 31, 493
MacConnell, D. J. 1968, ApJS, 16, 275
Mathews, W. G. 1969, ARA&A, 7, 69
Matthews, H. E. 1982, in Regions of Recent Star Formation, ed. R. S. Roger & P. E. Dewdney (Dordrecht: Reidel), 31
Oort, J. H., & Spitzer, L., Jr. 1955, ApJ, 216, 6
Panagia, N. 1973, AJ, 78, 929
Reipurth, B. 1983, A&A, 117, 183
Rossano, G. S., Angerhofer, P. E., & Grayzeck, E. J. 1980, AJ, 85, 716
Rossano, G. S., Grayzeck, E. J., & Angerhofer, P. E. 1983, AJ, 88, 1835
Spitzer, L., Jr. 1968, in Stars and Stellar Systems, Vol. 7, Nebulae and Interstellar Matter, ed. B. M. Middlehurst & L. H. Aller (Chicago: Univ. Chicago Press), 1
Sugitani, K., Fukui, Y., Mizuno, A., & Ohashi, N. 1989, ApJ, 342, L87
Sugitani, K., Fukui, Y., Ogawa, H., & Kawabata, K. 1986, ApJ, 303, 667
Taylor, D. K., & Dickman, R. L. 1988, in Molecular Clouds in the Milky Way and External Galaxies, ed. R. L. Snell & J. S. Young (Heidelberg-Verlag), 193
Thronson, H. A., Lada, C. J., & Hewagama, T. 1985, ApJ, 297, 662
Wootten, A., Sargent, A., Knapp, G., & Huggins, P. J. 1983, ApJ, 269, 147
Yang, J., Fukui, Y., Umemoto, T., Ogawa, H., & Chen, H. 1990, ApJ, 362, 538
Yang, J., Umemoto, T., Iwata, T., & Fukui, Y. 1991, ApJ, 373, 137